

<https://doi.org/10.1038/s44296-025-00072-w>

Toward tough and sustainable hydrogel-cement composites via biomineralization-inspired strategy

Han Wang¹, Yanchun Miao¹, Taotao Feng¹, Junlin Lin¹, Guoxing Sun², Zeyu Lu¹✉ & Jinyang Jiang¹

Enhancing the toughness of cement-based materials is key to extending their service life, reducing carbon emissions, and achieving sustainable development of the building materials industry. Drawing inspiration from the biomineralization in nature, a novel hydrogel-cement composite with an interpenetrating organic-inorganic structure was developed, followed by a rapid polymerization to pre-construct a continuous organic network, and a sequential deposition of inorganic cement hydrates on that, in order, thereby endowing the obtained composites with a honeycomb-like porous structure. Compared with normal cement paste, the hydrogel-cement composites (hydrogel content: 2.4–13.7 wt%) showed more than 30 times higher flexural toughness, and 60% increase in compressive strength. Besides, the composites exhibited high porosity characteristics consisting of closed micropores, which contributed to the 90% lower thermal conductivity of the composites than normal cement paste. In conclusion, these findings open a new window to toughen and functionalize cement-based materials with hydrogels using a biomineralization-inspired strategy.

The intrinsic quasi-brittleness of cement-based materials poses deformation and cracking risks during the service, which plays a negative role in the sustainable development of the building materials industry^{1,2}. Normally, organic polymers with excellent strength and toughness, including fibers, emulsions, rubber, etc., have been widely used as reinforcing components to toughen cement-based materials^{3,4}. Nevertheless, the toughening efficiency is greatly limited by the agglomeration of polymers due to the strong electrostatic interaction⁵, in which the agglomerated polymers act as defects rather than reinforcing phases⁶. Recently, an in-situ polymerization method has been proposed to address the agglomeration problem⁷, in which the polymer monomers are initially dissolved in water, followed by thorough stirring to achieve a uniform distribution of the monomer in cement slurry⁸. As cement hydration progresses, free radicals are gradually generated from polymer monomers and combine through covalent bonds, resulting in the formation of uniformly dispersed polymer in the cement matrix. Shao and Wu et al.^{9,10} summarized that the toughness of cement paste and mortar can be increased by 30–140% via in-situ polymerization method, without introducing defects or negatively impacting other performance of cement-based materials. Therefore, it exhibited great potential to improve the toughness of cement-based materials.

To our knowledge, in the in-situ polymerization method, the interconnection degree of polymers in the cement matrix plays an important role

in the corresponding toughening efficiency¹¹. Nevertheless, the formation of a continuous polymer network is usually inhibited by cement hydration¹². Specifically, it relies on the continuously dispersed water in the cement slurry, which serves as the medium for monomer polymerization and polymer chain interconnection. However, due to the consumption of water during cement hydration, the continuously dispersed water shrinks and separates into small droplets under the influence of surface tension^{13,14}. This phenomenon reduces the possibility of polymer chains interconnection, thereby preventing the formation of a continuous polymer network. In that case, how to generate a continuous polymer network in the cement matrix remains unclear.

The biomineralization process offers valuable insights into the construction of a continuous polymer network in inorganic materials^{15,16}, which requires the prior formation of a polymer network, followed by the attachment of inorganic particles onto it. A series of organic-inorganic composites with exceptional toughness, including bone, shell and pearl, are naturally constructed via biomineralization^{17,18}. It is noteworthy that hydroxyapatite, the main inorganic component in biomineralization, is a strong, low-solubility material consisting of $(\text{PO}_4)^{2-}$ coordinated with Ca^{2+} . Similarly, the main hydration product of cement, calcium silicate hydrate (C-S-H), exhibits a comparable strength, solubility to hydroxyapatite, as well as a similar structural, composed of $(\text{SiO}_4)^{2-}$ coordinated with Ca^{2+} ^{19,20}.

¹State Key Laboratory of Engineering Materials for Major Infrastructure, School of Materials Science and Engineering, Southeast University, Nanjing, China. ²Joint Key Laboratory of the Ministry of Education, Institute of Applied Physics and Materials Engineering, University of Macau, Taipa, Macau, SAR, China.

✉ e-mail: 101012819@seu.edu.cn

However, unlike biomineralization, rapidly forming a gel network in cement paste before the formation of hydrates remains challenging. In previous research, the polymer network normally slowly formed within 12–48 h^{21,22} after mixing. This is attributed to the high concentration of OH⁻ in the cement slurry, which can react with S₂O₈²⁻ in ammonium persulfate—the most commonly used polymerization initiator²³, thereby inhibiting monomer polymerization and delaying network formation. Consequently, strategies for rapidly forming polymer networks in cement slurries with high alkalinity and ionic strength need further investigation.

Herein, the current study developed the biomineralization-inspired hydrogel-cement composites with exceptional toughness. A pre-association strategy between monomers and initiators was adopted to avoid the inhibitory effect of OH⁻ in the cement pore solution on the polymerization reaction. SEM results indicated that a continuous hydrogel network was formed within the cement matrix before the initiation of cement hydration (Fig. 1)²⁴. This network subsequently induced the deposition of cement hydrates onto its surface (Fig. 1d, e), leading to the formation of honeycomb-like porous structure composed of closed pores. As a result, compared with normal cement paste, the hydrogel-cement composites showed 3195% and 60% enhancement in flexural toughness and

compressive strength. MIP, TG, and thermal simulation results demonstrated that the closed porous structure contributed to the highly thermal insulation performance of composites. Furthermore, FT-IR and NMR analyzes confirmed the good interfacial compatibility between the hydrogel and cement hydrates. In summary, this research provides a novel perspective on toughening cement-based materials with hydrogels via a biomineralization-inspired strategy.

Results and discussion

Microstructure

The formation of hydrogel network and the sequential deposition of cement hydrates are investigated, as shown in Fig. 2. It can be seen that the continuous hydrogel network is rapidly constructed within 2 min after the mixing of all raw materials (Fig. 2a and S.1c, d). Compared to the slow rate of conventional in-situ polymerization (12–48 h)^{21,22}, this rapid polymerization of hydrogel overcomes the inhibition effects of cement hydration to the formation of a continuous polymer network. On the one hand, the consumption effects of OH⁻ on S₂O₈²⁻ are inhibited: The hydrogel monomer and initiator are blended in aqueous solution before mixing with cement particles, which avoids the consumption effects of OH⁻ released by cement

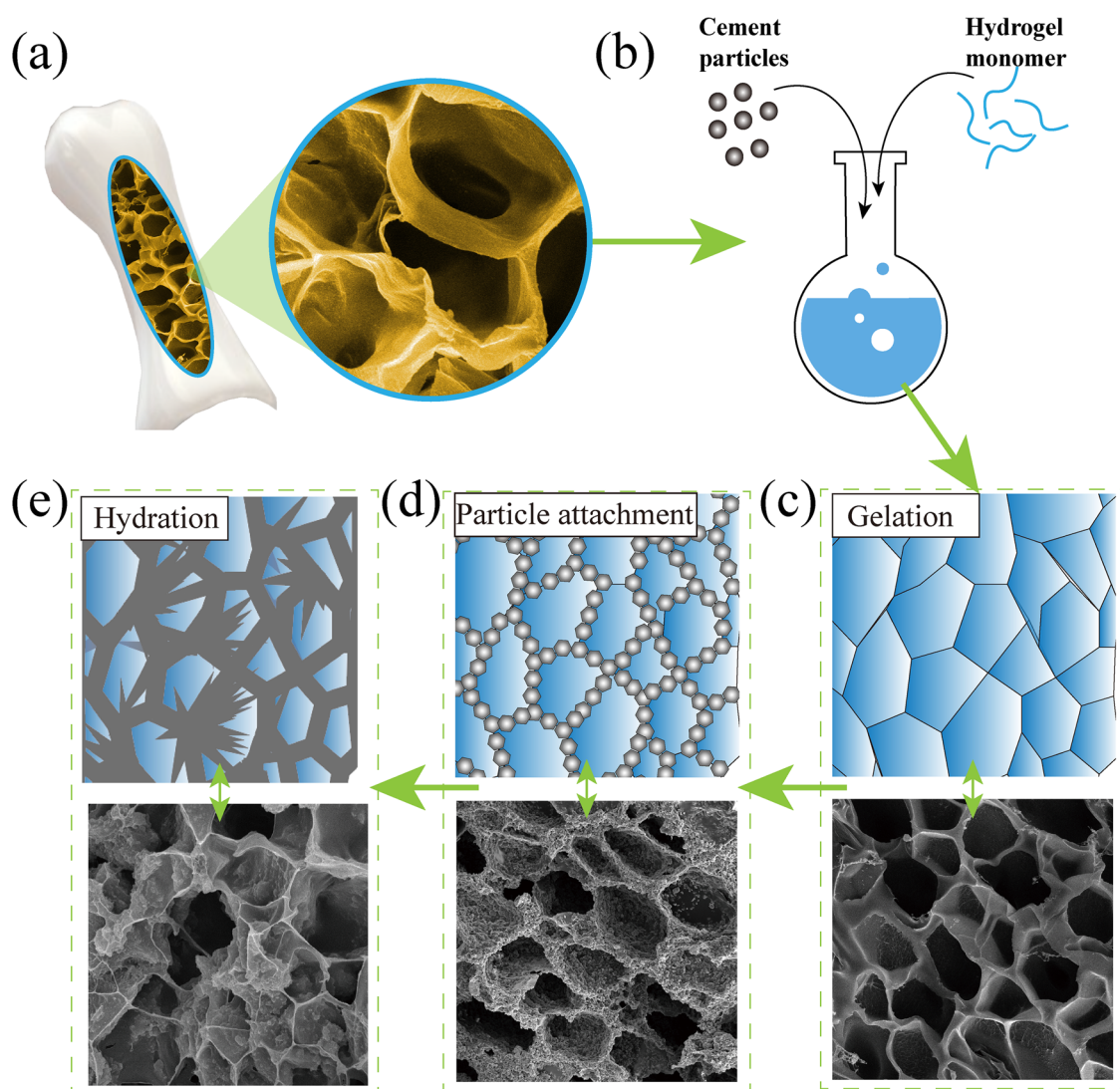


Fig. 1 | Schematic illustration. **a** Structure of spongy bone. **b** Preparation process of composites. **c** In-situ polymerization of hydrogel monomers within the cement matrix forms a continuous three-dimensional polymer network. **d** Attachment of cement particles on hydrogel network. **e** After polymerization, water is gradually

released from hydrogel and reacts with the adhered cement particles, leading to the formation and deposition of cement hydration products on the network surface. Throughout this process, the integrity of the three-dimensional hydrogel network is still maintained.

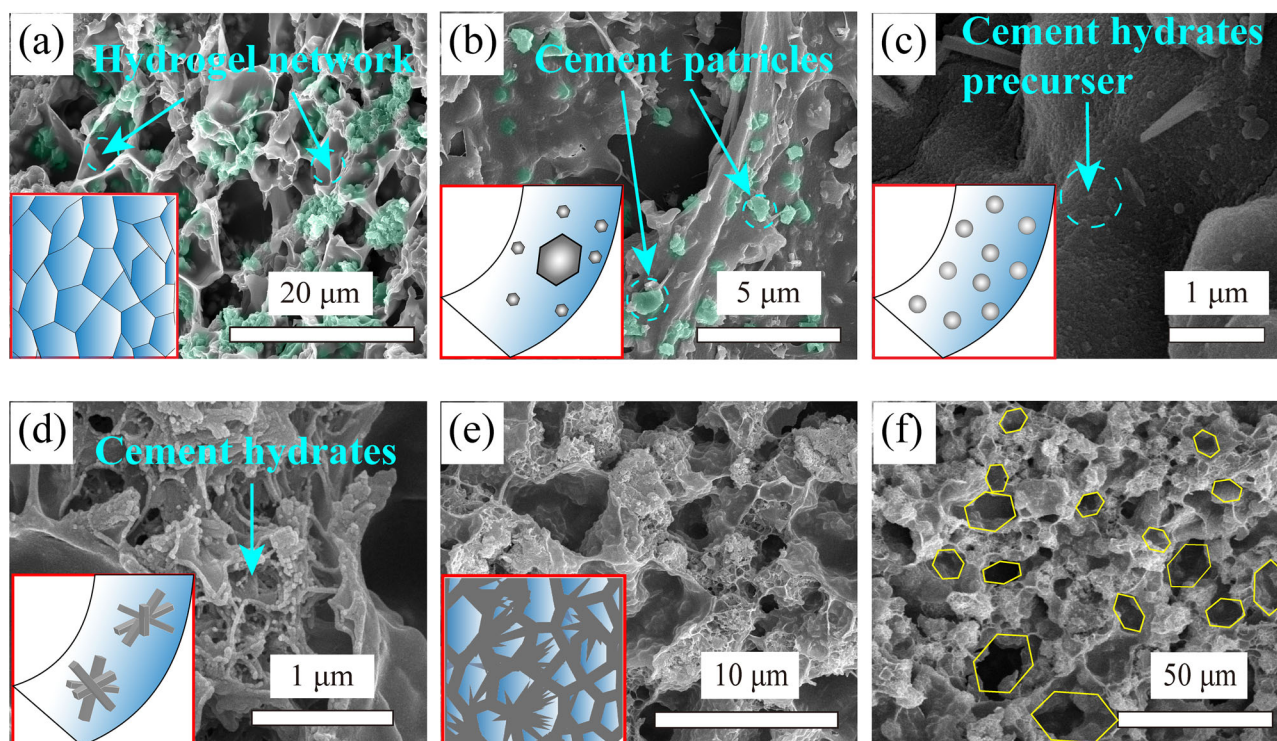


Fig. 2 | Scanning Electron Microscope (SEM) images of composites. **a** Rapid in-situ polymerization of hydrogel occurs within 2 min after mixing, forming a continuous hydrogel network; meanwhile, cement particles adhere on the surface of the hydrogel network. **b** After 1 day of mixing, water is gradually released from the hydrogel driven by humidity difference, promoting the localized dissolution of

cement particles on its surface. **c** After 3 days of mixing, cement hydrates precursors are observed on the surface of hydrogel network. **d** After 28 days of mixing, continued ion accumulation leads to the transformation of precursors into crystallized cement hydrates along the hydrogel skeleton. **e, f** The porous structure of composites in different scales, taken after 28 days of mixing.

particles on initiator anion ($\text{S}_2\text{O}_8^{2-}$), therefore accelerating the formation rate of polymer chains²³. This process facilitates a faster release of free radicals from the monomer, which in turn accelerates the polymerization of polymer chains. On the other hand, the hindrance of cement particles to polymer chain interaction is avoided: the dosage of cross-linking agent is optimized to increase the possibility of polymer chains contacting with each other in cement slurry, which also accelerates the formation of continuous hydrogel network within the cement.

After that, the continuous hydrogel network plays a template role to induce sequential deposition of cement hydrates, which can be divided into three stages, as depicted in Fig. 2b–e. Stage I-Attachment: due to the formation of hydrogen bonds between the polar functional groups (e.g., $-\text{OH}$, $-\text{COOH}$, $-\text{CONH}_2$) of the organic molecular chains and the hydroxylated surfaces of cement hydration products, along with van der Waals forces arising from molecular proximity^{25,26}, cement particles are more likely to attach to the hydrogel surface. Stage II-Dissolution: during the polymerization process of hydrogel, the free water in cement slurry is absorbed by the hydrophilic groups ($-\text{COOH}$ and $-\text{OH}$) on hydrogel. Then, driven by the humidity difference between the inside and outside of hydrogel, the water slowly released from hydrogel to cement particles. This process promotes the dissolution of cement particles on the surface of hydrogel (Fig. 2b)²⁷. Stage III-Deposition: according to classical heterogeneous nucleation theory²⁸, the skeleton of hydrogel provides extra nucleation sites that reduce the free energy barrier for the crystallization of cement hydrates precursors, inducing their deposition onto the skeleton (Fig. 2c)^{29,30}. Subsequently, these hydrate precursors transform into crystallized hydrates during the hydration process (Fig. 2d). The aforementioned process facilitates the deposition of cement hydrates on hydrogel network. As a result, the pore shape and distribution characteristics of hydrogels are inherited by composites after cement hydration. Consequently, as shown in Fig. 2f, the pores in composites are uniformly distributed closed pores with honeycomb-like shape.

Mechanical properties

The continuous hydrogel network with honeycomb-like pore structure benefits to the mechanical enhancement of cement paste, as shown in in Fig. 3a–d. Firstly, the flexural strength (Fig. 3a) of the hydrogel-cement composites is 11–24 MPa and 13–28 MPa at 7 days and 28 days, respectively, which is 13–158% higher than that of *Ref.* (pure cement paste without hydrogel). Besides, through the comparison of the area below the stress–strain curve (Fig. 3b), it can be seen the flexural toughness of the composites is higher than *Ref.* by 231–3195% at 28 days. Such a remarkable mechanical enhancement is related to the network effectively preventing the generation and propagation of cracks under loading, thus contributing to the toughness enhancement of composites. Besides, Pan et al.³¹ indicated that compared to the separated polymer fragments after in-situ polymerization, the continuous hydrogel network increases the contact area with the cement matrix, and thus avoids the interfacial stripping of hydrogel/matrix during the loading process. This further optimizes the energy absorption capability of the hydrogel, thereby enhancing the flexural strength.

Notably, the flexural strength of the composites increases with the rising hydrogel content, which is associated with the progressive reduction in pore size, as shown in Fig. S2c–e. The smaller pores help to mitigate stress concentration, thereby enhancing the strength³². Besides, the strength initially rises but subsequently declines with the increasing cement proportion. This reduction suggests that while increasing the cement content enhances flexural strength by generating more hydrates, an excessive amount disrupts the integrity of the hydrogel network³³, ultimately reducing the overall strength of the composite. These insights pave the way for future research aimed at optimizing the composition of composites to achieve even higher flexural strength.

As shown in Fig. 3c, the hydrogel-cement composites exhibit high compressive strength (16–59 MPa and 32–62 MPa at 7 days and 28 days, respectively). In particular, the compressive strength of H3H2 is higher than

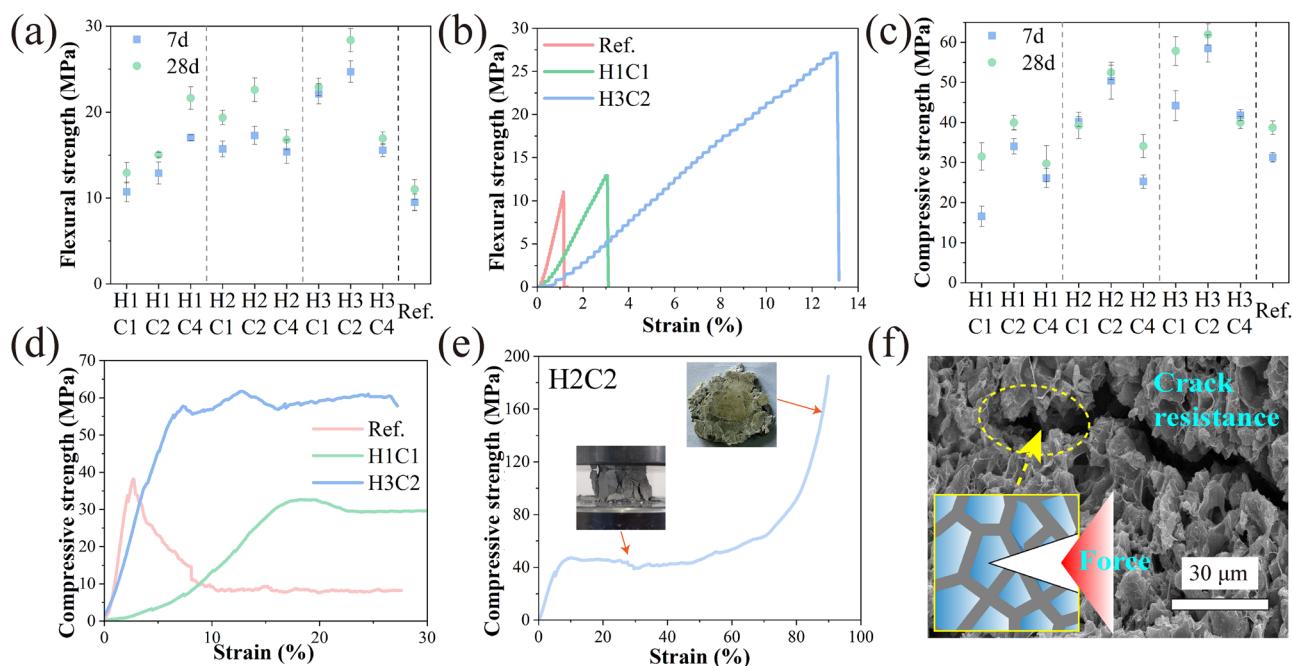


Fig. 3 | Mechanical properties. **a** Flexural strength of composites and Ref. at 7 days and 28 days. Error bars represent the standard deviation based on three specimens for flexural strength. **b** Flexural strength-strain curve of composites. **c** Compressive strength of composites and Ref. at 7 days and 28 days. Error bars represent the

standard deviation based on six specimens for compressive strength.

d, e Compressive strength-strain curve of composites. **f** Schematic illustration of porous structure preventing the crack propagation.

that of Ref. by 60%. It can be seen that the strength increases with the rising hydrogel/cement content, following a similar trend to that observed in the flexural strength. In addition, the compressive strength of the composites increased with decreasing water-to-cement ratio, primarily due to the reduced porosity and the resulting denser microstructure of the matrix. Figure 3d, e illustrates that, compared with Ref., the composites show plastic rather brittle deformation characteristics under compression. The special deformation-tolerant behavior is mainly attributed to the honeycomb-like porous structure. First, during the loading process, the crack tips can be blunted by the honeycomb-like pores of composites, thereby reducing the stress concentration at the crack tip and hindering further crack propagation³⁴. Additionally, the fracture energy can be consumed by the deformation of the pores, as shown in Fig. 3f, which jointly triggers the plastic deformation characteristics of the composites³⁵. Notably, with the increasing strain from 10 to 80%, the strength of composites is correspondingly increased from 47 to 86 MPa. The result shows that the composites can maintain structural integrity under large deformation conditions, which is beneficial for the stability of building materials serving in extreme conditions of high seismic intensity, ground stress and water pressure, etc.

Interaction between the hydrogel and cement hydrates

Given its excellent mechanical performance, H₂C₂ is selected for in-depth analysis to investigate the interactions between hydrogel and cement hydrates, as shown in Fig. 4. The characteristic peaks of hydrogel-cement composites at 3437 cm⁻¹, 2970 cm⁻¹, 1650 cm⁻¹ and 816 cm⁻¹ correspond to -OH, -CH, -NH, and C=O in hydrogel, respectively. Additionally, the characteristic peaks with high intensity at 975 cm⁻¹ are assigned to Si-O in C-S-H. Notably, the O-H peaks at 3437 cm⁻¹ in composites are wider than those in Ref. (Fig. S.3a) and hydrogel, suggesting the formation of extra hydrogen bonds in composites. This phenomenon is ascribed to the interaction between -COO⁻ in the hydrogel and cations (Ca²⁺, Al³⁺) in cement hydrates, which confirms the good interfacial compatibility between hydrogel and cement hydrates^{23,36}. The solid-state 1H NMR spectra further corroborate this finding, as shown in Fig. 4 (b). The characteristic peaks at 4.6 ppm and 23.6 ppm correspond to -CH in the hydrogel^{37,38} and -OH in

cement hydrates³⁹, respectively. Compared to the pure hydrogel, the chemical shift of the -CH peak at 4.6 ppm indicates an increased degree of cross-linking in the composites (Fig. 4c). This is beneficial for enhancing the continuity of hydrogel within the cement matrix, a factor that is crucial for the corresponding toughening efficiency to cement-based materials.

In addition, the phase compositions and microstructure of hydrogel-cement composites are investigated, as shown in Fig. 5d-f. Firstly, it can be seen that the crystal size of plate-like hydrates (Ca(OH)₂) in composites is larger than that in Ref. (S.3d-f). These Ca(OH)₂ crystals act as short fibers by bridging microcracks and facilitating load transfer across the matrix, thereby enhancing the flexural strength of the composite³⁴. The increase in Ca(OH)₂ particle size is attributed to the porous structure of the hydrogel network, which provides ample space for Ca(OH)₂ growth. This, in turn, helps to reduce local supersaturation, thereby increasing the corresponding grain size. Notably, the larger Ca(OH)₂ no longer deposits on the surface of hydrogel network but intertwines with hydrogel network, forming an interpenetrating structure (Fig. 4d). According to⁴⁰, this structure enhances the adhesion between the crystal interlayer of Ca(OH)₂ through hydrogen bonding, thereby preventing interlayer slippage-induced structural failure and strength loss⁴¹, as depicted in Fig. 4e. Besides, the content of C-S-H gels in hydrogel-cement composites is higher than that in Ref. As the main contributor to the strength of cement-based materials, the increment of C-S-H gels content is conducive to the mechanical enhancement of the composites, which is consistent with the results presented in section "Mechanical properties". Therefore, the above results prove that the synergistic effects of hydrogel and cement hydrates are conducive to the improvement of hydrogel continuity and the increase of cement hydrates content. However, the effects of variations in hydrogel and cement content on phase composition and microstructure, as well as their correlation with mechanical strength, remain unclear and should be investigated in the future.

Pore structure and thermal properties

As shown in Fig. 5a, the porosity of different composites ranges from 24 to 67%, which is 60–347% higher than that of Ref. (15%). It is evident that the increasing hydrogel content leads to a reduction in composites porosity,

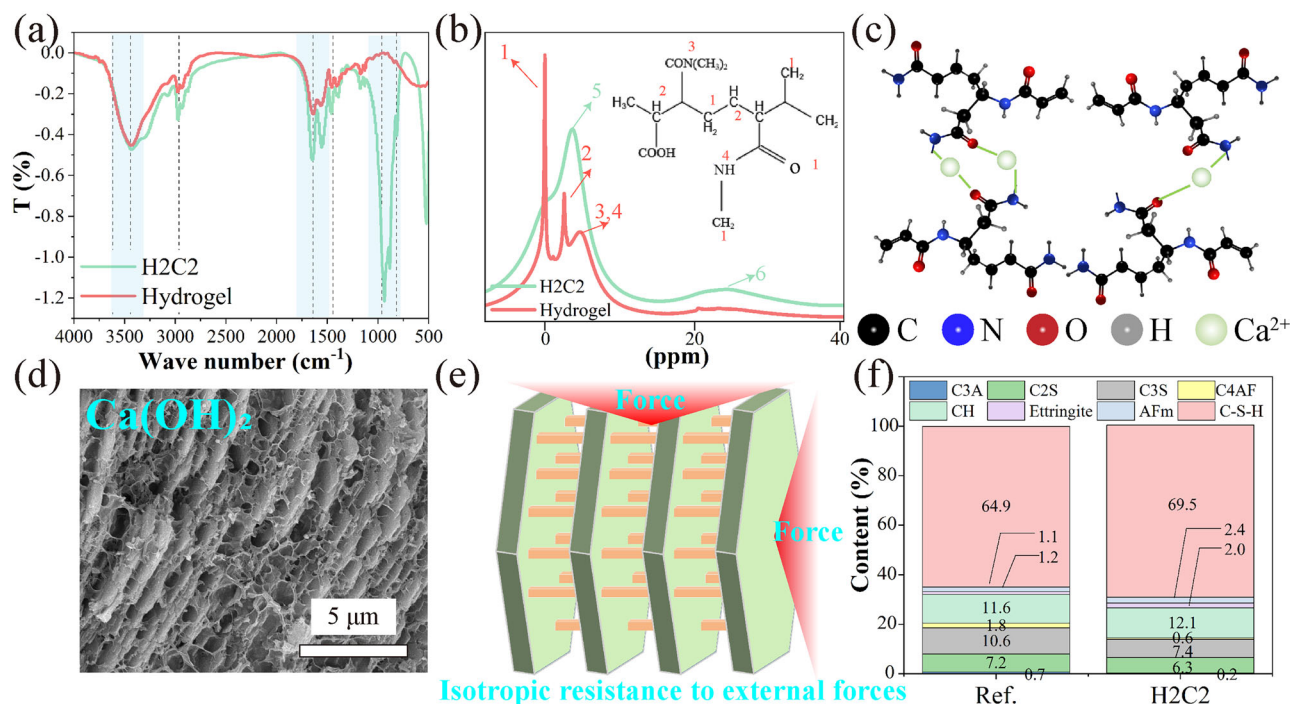


Fig. 4 | Characterization of the interaction between hydrogel and cement hydrates. **a** FT-IR spectra of composites. **b** Solid-state ¹H NMR spectra of composites. **c** Schematic diagram of the interaction between hydrogel and Ca²⁺ released

by cement. **d** Microstructure of composites. **e** Schematic illustration of interpenetrating structure in Ca(OH)₂-hydrogel composites. **f** Phase composition of composites.

which accounts for the enhanced compressive and flexural strength due to a denser microstructure and reduced stress concentrations from pore defects. However, lower porosity compromises the lightweight and thermal insulation performance of the composites. Therefore, achieving an optimal balance between mechanical strength and thermal insulation is essential. Among the various mixtures, H2C2 demonstrates a favorable compromise between strength and lightweight properties. Consequently, its pore structure, thermal conductivity, and thermal stability are systematically investigated.

According to Fig. 5b, the MIP results indicate that the pore size distribution of the composites primarily ranges from 10 to 100 nm, which is attributed to the stack gaps among cement hydrates. It is noteworthy that MIP test fails to capture the micro-scale pores visible in scanning electron microscopy (SEM) images (Fig. 2). This phenomenon suggests that the micro-pores in composites are closed pores, which cannot be invaded by mercury thus undetectable by MIP test. Compared to connected pores, closed pores can effectively reduce thermal convection and radiation⁴², thereby decreasing the thermal conductivity of composites, which is investigated in the following part.

As shown in Fig. 5c, the thermal conductivity of composites (0.14 W/m K) is lower than that of Ref. by 90%, and commercial insulating building materials such as rubber, foamed concrete, and wood (0.16–0.85 W/m K)². Additionally, after being heated from the bottom (200 °C) for 30 min, the temperature of the upper surface of the composite and Ref. is 50 °C and 140 °C, respectively (Fig. 5d). The above results indicate the good thermal insulation performance of the composite due to its porous structure majorly composed of closed pores. Besides, the thermal stability of composites is investigated by TG analysis. As shown in Fig. 5e, the weight loss of composites in 100–150, 300–350, 350–430 °C corresponds to the degradation of C–S–H gels, hydrogel and Ca(OH)₂ in the composites. The result shows that 56–63% mass of the composites is maintained after calcination at 1000 °C, indicating good thermal stability and structural integrity at high temperature. Additionally, Fig. 5f illustrates that the dielectric constant of the composite is 40–60% lower than that of conventional cement-based materials. This reduction is attributed to the closed pores in composites,

which facilitate the scattering and attenuation of electromagnetic waves. Therefore, the composites exhibit both high thermal insulation and wave absorption capabilities. This multifunctionality positions the hydrogel-cement composites as a promising solution for various engineering challenges, such as thermal management and sound attenuation⁴³.

Discussion

Drawing inspiration from the biomineralization in nature, a tough and sustainable hydrogel-cement composite was developed in the current research, the main conclusions are drawn as follows:

- A novel strategy was proposed for the first time to realize the construct of continuous polymer network within a cement matrix, followed by a rapid polymerization to pre-construct a continuous organic network, and a sequential deposition of inorganic cement hydrates on that in order, thereby endowing the obtained composites with a honeycomb-like porous structure.
- The formation of continuous hydrogel network resulted in remarkable improvements in the toughness of hydrogel-cement composites. Compared with normal cement paste, the developed composites showed a 3195% enhancement in flexural toughness and a transform in compressive failure from brittleness to ductile behavior, with 83% increase in compressive strength as strain rose from 10 to 80%.
- The Ca²⁺ released by cement contributed to the increasing cross-linking degree of hydrogel, and the hydrogel provided more water for cement therefore increasing the content of C–S–H gels. The synergistic effect between hydrogel with cement is conducive to the enhancement of composite's mechanical strength.
- The composites exhibited high porosity (67%) characteristics consisting of closed micropores, which contributed to the 90% lower thermal conductivity of composites than normal cement paste.

Methods

Materials

The analytical-grade monomer (N-isopropylacrylamide (NIPAm), sodium acrylate (SA)), crosslinkers (N, N-methylenebisacrylamide

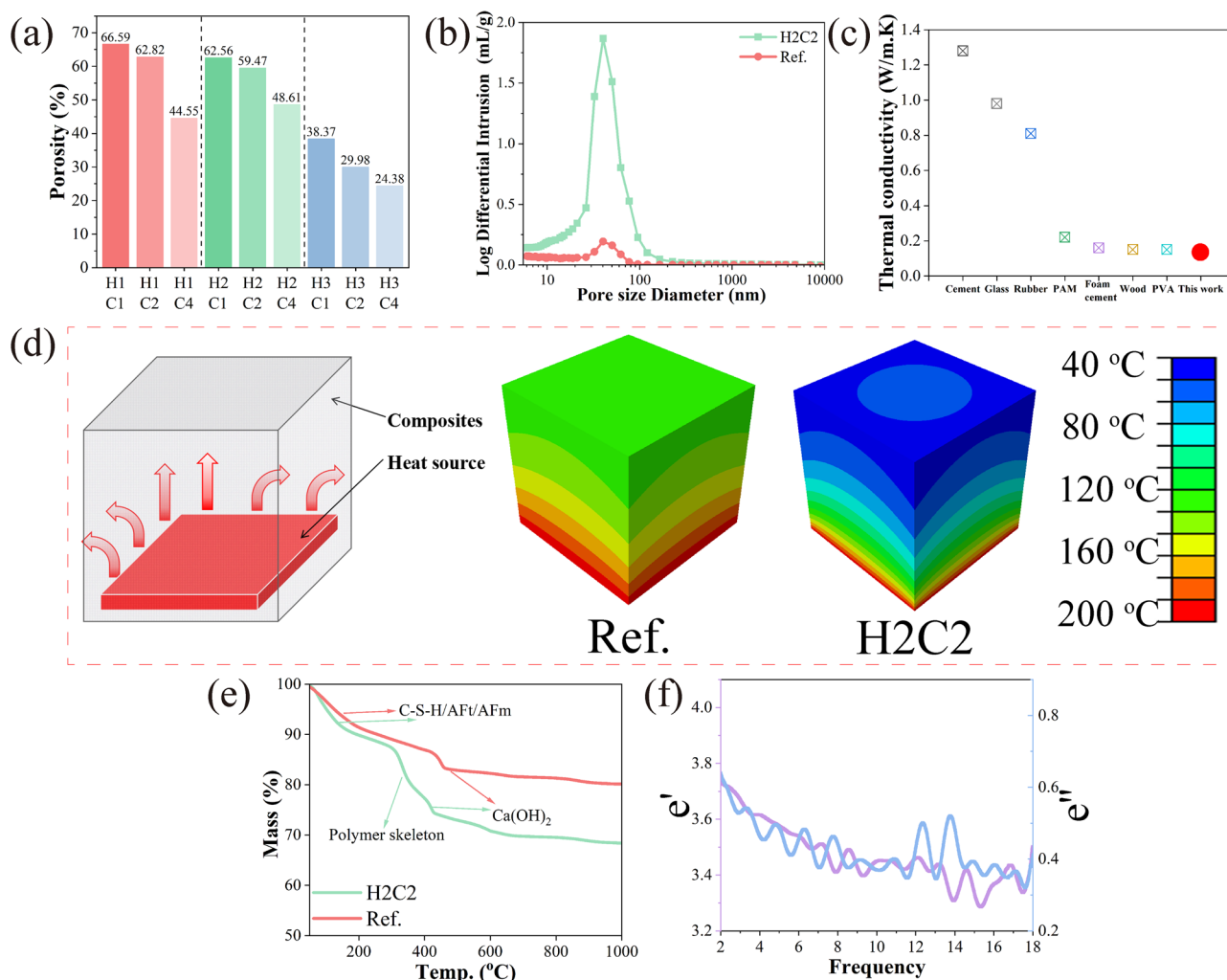


Fig. 5 | Pore structure and thermal properties of composites. a, b Porosity and pore size distribution. **c** Thermal conductivity of different building materials. **d** Simulation of insulation performance. **e** Thermal stability of composites. **f** Wave adsorption of composites.

(Bis)), initiators (potassium persulfate (APS)) and catalyzer (N, N, N'-tetramethylethylenediamine (TEMED)) were procured from Shanghai Macklin Biochemical Co., Ltd. Additionally, the ground P-I cement ($D(50) = 9.6 \mu\text{m}$, $D(90) = 18.2 \mu\text{m}$) was provided by China Shanshui Cement Group. The phase composition of cement was listed in S-Table 1 in Supplementary Files.

The mix designs for different composites are shown in Table 1. In this composite, the content of hydrogel monomers determines the crosslinking density of the polymer network, thereby affecting the pore size of the composite. Meanwhile, the cement content governs the formation of hydrates, thus affecting the strength. Accordingly, mixtures with varying contents of hydrogel monomers and cement were designed. Three hydrogel monomer dosages (5, 10, and 20 g) were investigated, corresponding to H1, H2, and H3, respectively. For each hydrogel dosage, three cement contents (25, 50, and 100 g) were tested, and labeled as C1, C2, and C4. The water content was kept constant at 100 g across all groups. This factorial design enabled a systematic evaluation of the effects of both hydrogel and cement contents on the composite properties. The fabrication process of hydrogel cement composites began with the sequential dissolution of hydrogel ingredients (NIPAm, SA, Bis, and APS) in deionized water. Subsequently, TEMED and cement particles were added with continuous stirring in the N_2 environment. The polymerization of hydrogel occurred swiftly within 2 min, and the solution was transformed into gel. After that, the composites were placed in a curing container maintained at 20°C and 95% RH until testing.

Characterization

Microstructure. The microstructure of composites is detected using a Scanning Electron Microscope (SEM, Navo Nano SEM450, Thermo Fisher Scientific, USA) operating at 15 kV with three spot sizes. The fresh cement paste, after 2 min of mixing, was rapidly frozen in liquid nitrogen for 2 min and subsequently freeze-dried at -50°C for 8 h. Then, the surface of dried specimens was coated with platinum to ensure good electrical conductivity during testing.

Mechanical strength. The compressive and flexural strength of composites at 7 days and 28 d were tested according to ASTM C513. For compressive strength testing, $\phi 20 \times 20 \text{ mm}$ cylindrical specimens with pre-capped load surfaces were used, while $10 \times 10 \times 50 \text{ mm}$ cuboid specimens were employed for flexural strength testing. 100 KN Mechanical Universal Testing Machine (UTM5105, SUNS, China) was used at defined loading rates: 2 mm/min for compressive strength and 1 mm/min for flexural strength. The load surface of composites was capped before the compressive strength. Averages of six and three replicate tests were used for compressive and flexural strength measurements, respectively. Notably, the difference in specimen size between this study and practical engineering applications warrants further investigation.

Interaction between cement particles and hydrogel. Before the test, composites were immersed in an isopropanol solution for 7 days to stop the cement hydration. Afterward, the composites were dried and then

Table 1 | Mixture design for different composites

Mixture ID	H1C1	H1C2	H1C4	H2C1	H2C2	H2C4	H3C1	H3C2	H3C4	Ref.
Cement (g)	25	50	100	25	50	100	25	50	100	100
Water (g)	100			100			100			100
NIPAm (g)	4			8			16			-
SA (g)	1			2			4			-
Bis (g)	0.1			0.2			0.4			-
APS (g)	0.05			0.1			0.2			-
TEMED (ml)	0.1			0.2			0.4			-

ground to pass through a 200-mesh sieve. Solid 1H NMR spectroscopy from Bruker (Neo 400WB, Germany) was adopted. Data analysis was performed using MestReNova Software. Fourier Transform Infrared Spectrometer (FT-IR) from Nicolet (Madison-WI, USA) was used to investigate the chemical functional groups of composites. Quantitative X-ray diffraction (QXRD) patterns are utilized to investigate the phase composition of composites, employing AXS D8 ADVANCE (Bruker, Germany) with CuK α radiation. α -Al₂O₃ was utilized as the internal standard for the QXRD test. The obtained results were analyzed using TOPAS software, and the content variation of clinker phase was detected for the cement hydration degree calculation according to ref. 44.

Thermal properties. The porosity of composites was obtained following the equation (1) in supplementary, in which the skeleton density and volume density were detected according to GB/T 208-2014. The thermal insulation simulation of composites was conducted using the heat transfer module of ABAQUS software according to Fick's second law. The heat source (200 °C) was set at the bottom of the specimen. The simulation parameters are shown in S-Table 2 in the Supplementary Files. The thermal stability of the composites below 1000 °C was evaluated by thermogravimetric analysis (TG, STA 449 F5, NETZSCH, Germany). Before the test, composites were placed in a vacuum oven at 40 °C for 72 h to remove free water. Approximately 50 mg of ground powder was then heated from 30 °C to 1000 °C at 10 °C/min under a nitrogen atmosphere. Besides, the electromagnetic wave absorption properties of the composites were measured using a vector network analyzer (E5071C, Agilent, USA) based on the coaxial transmission line method. Bulk samples were selected for measurement in the frequency range of 1–18 GHz.

Data availability

The data are available on request to the corresponding author.

Received: 22 April 2025; Accepted: 26 June 2025;

Published online: 03 September 2025

References

- Birchall, J. D., Howard, A. J. & Kendall, K. Flexural strength and porosity of cements. *Nature* **289**, 388–390 (1981).
- Du, F. et al. Bioinspired super thermal insulating, strong and low carbon cement aerogel for building envelope. *Adv. Sci.* **10**, 2300340 (2023).
- Fan, L. et al. A review on the modification mechanism of polymer on cement-based materials. *J. Mater. Res. Technol.* **26**, 5816–5837 (2023).
- Pang, B. et al. The interpenetration polymer network in a cement paste–waterborne epoxy system. *Cem. Concr. Res.* **139**, 106236 (2021).
- Lu, Z., Yao, J. & Leung, C. K. Y. Using graphene oxide to strengthen the bond between PE fiber and matrix to improve the strain hardening behavior of SHCC. *Cem. Concr. Res.* **126**, 105899 (2019).
- Hernández-Cruz, D. et al. Multiscale characterization of chemical-mechanical interactions between polymer fibers and cementitious matrix. *Cem. Concr. Compos.* **48**, 9–18 (2014).
- Yin, B. et al. Mechanical properties and micro-mechanism of cement-based materials strengthened by in-situ organic-inorganic polymerization. *Cem. Concr. Compos.* **142**, 105202 (2023).
- Yin, B. et al. Performance cement-based composite obtained by in-situ growth of organic-inorganic frameworks during the cement hydration. *Constr. Build. Mater.* **336**, 127533 (2022).
- Shao L., et al. In-situ polymerization-modified cement composites: a critical review. *Constr. Build. Mater.* **449**, 138294 (2024).
- Wu, K., Long, J., Qing, L. & De Schutter, G. Recent advance of monomer in-situ polymerization modified cement-based materials. *Constr. Build. Mater.* **432**, 136542 (2024).
- Liang, R., Liu, Q., Hou, D., Li, Z. & Sun, G. Flexural strength enhancement of cement paste through monomer incorporation and in situ bond formation. *Cem. Concr. Res.* **152**, 106675 (2022).
- Chen, B. M., Qiao, G., Hou, D. S., Wang, M. H. & Li, Z. J. Cement-based material modified by in-situ polymerization: From experiments to molecular dynamics investigation. *Compos. Part B* **194**, 108036 (2020).
- Guo, S. Y., Zhang, X., Chen, J. Z., Mou, B. & Ren, J. Mechanical and interface bonding properties of epoxy resin reinforced Portland cement repairing mortar. *Constr. Build. Mater.* **264**, 120715 (2020).
- Wang, H. et al. Hydrogel-guided dispersion strategy for enhancing the toughening efficiency of liquid polymers in cement paste. *Cem. Concr. Res.* **195**, 107926 (2025).
- Dai, H. et al. Advanced composites inspired by biological structures and functions in nature: architecture design, strengthening mechanisms, and mechanical-functional responses. *Adv. Sci.* **10**, 2207192 (2023).
- Yao, S. et al. Biomineralization: from material tactics to biological strategy. *Adv. Mater.* **29**, 1605903 (2017).
- Kim, J. H. & Min, K. I. Assembly and biomineralization of polymorphic gold–peptide superstructures using tyrosine-rich short peptides. *Adv. Funct. Mater.* **33**, 2210196 (2022).
- Deng, Z., Jia, Z. & Li, L. Biomineralized materials as model systems for structural composites: intracrystalline structural features and their strengthening and toughening mechanisms. *Adv. Sci.* **9**, 2103524 (2022).
- Zhang, Z., Wang, X., Wang, H. & Zhao, J. Removal of Pb(II) from aqueous solution using hydroxyapatite/calcium silicate hydrate (HAP/C-S-H) composite adsorbent prepared by a phosphate recovery process. *Chem. Eng. J.* **344**, 53–61 (2018).
- Duque-Redondo, E., Bonnaud, P. A. & Manzano, H. A comprehensive review of C-S-H empirical and computational models, their applications, and practical aspects. *Cem. Concr. Res.* **156**, 106784 (2022).
- Liang, C. P., Hao, L. C., Yu, H. Z. & Yuanfeng, Z. A comprehensive review on polyurethane modified asphalt: mechanism, characterization and prospect. *J. Road. Eng.* **3**, 315–335 (2023).

22. Chen, S. et al. An experimental and theoretical study of biomimetic cement-epoxy resin composites: structure, mechanical properties, and reinforcement mechanisms. *Compos. Part A* **185**, 108297 (2024).
23. Sun, G., Li, Z., Liang, R., Weng, L. T. & Zhang, L. Super stretchable hydrogel achieved by non-aggregated spherulites with diameters <5 nm. *Nat. Commun.* **7**, 12095 (2016).
24. Song, X. F., Chu, Y. Y. & Zhao, H. X. Water-swellable, tough, and stretchable inorganic-organic sulfoaluminate cement/polyacrylamide double-network hydrogel composites. *J. Appl. Polym. Sci.* **136**, 47905 (2019).
25. Kontturi, E. et al. Advanced materials through the assembly of nanocelluloses. *Adv. Mater.* **30**, 1703779 (2018).
26. Thoniyot, P., Tan, M. J., Karim, A. A., Young, D. J. & Loh, X. J. Nanoparticle-hydrogel composites: concept, design, and applications of these promising, multi-functional materials. *Adv. Sci.* **2**, 1400010 (2015).
27. Scherer, G. W., Zhang, J. & Thomas, J. J. Nucleation and growth models for hydration of cement. *Cem. Concr. Res.* **42**, 982–993 (2012).
28. Aretxabaleta, X. M., Lopez-Zorrilla, J., Etxebarria, I. & Manzano, H. Multi-step nucleation pathway of C-S-H during cement hydration from atomistic simulations. *Nat. Commun.* **14**, 7979 (2023).
29. Pan, Z., Yao, L., Zhai, J., Yao, X. & Chen, H. Interfacial coupling effect in organic/inorganic nanocomposites with high energy density. *Adv. Mater.* **30**, 1705662 (2018).
30. Zhang, Z. D., Scherer, G. W. & Bauer, A. Morphology of cementitious material during early hydration. *Cem. Concr. Res.* **107**, 85–100 (2018).
31. Pan, Z., Yao, L., Zhai, J., Yao, X. & Chen, H. Interfacial coupling effect in organic/inorganic nanocomposites with high energy density. *Adv. Mater.* **199**, 1705662 (2018).
32. Jin, S., Zhou, J., Zhao, X. & Sun, L. Quantitative relationship between pore size distribution and compressive strength of cementitious materials. *Constr. Build. Mater.* **273**, 121727 (2021).
33. Kim, S. et al. In situ mechanical reinforcement of polymer hydrogels via metal-coordinated crosslink mineralization. *Nat. Commun.* **12**, 667 (2021).
34. Qi, C., Jiang, F. & Yang, S. Advanced honeycomb designs for improving mechanical properties: a review. *Compos. Part B* **227**, 109393 (2021).
35. Wang, F. et al. Wood-inspired cement with high strength and multifunctionality. *Adv. Sci.* **8**, 2000096 (2021).
36. Krystek, M. et al. High-performance graphene-based cementitious composites. *Adv. Sci.* **6**, 1801195 (2019).
37. Arens, L., Barther, D., Landsgesell, J., Holm, C., Wilhelm, M. Poly(sodium acrylate) hydrogels: synthesis of various network architectures, local molecular dynamics, salt partitioning, desalination and simulation. *Soft Matter* **15**, 9949–9964 (2019).
38. Hou, F. et al. Self-healing hydrogel with cross-linking induced thermo-response regulated light emission property. *Colloids Surf. B* **183**, 110441 (2019).
39. Guo, H. et al. Quantitative phase analyses of biomedical pyrophosphate-bearing monetite and brushite cements by solid-state NMR and powder XRD. *Ceram. Int.* **46**, 11000–11012 (2020).
40. Knapen, D. V. G. E. Cement hydration and microstructure formation in the presence of water-soluble polymers. *Cem. Concr. Res.* **39**, 6–13 (2009).
41. Picker, A. et al. Mesocrystalline calcium silicate hydrate: A bioinspired route toward elastic concrete materials. *Sci. Adv.* **3**, e1701216 (2017).
42. Liu, H. & Zhao, X. Thermal conductivity analysis of high porosity structures with open and closed pores. *Int. J. Heat. Mass Transf.* **183**, 122089 (2022).
43. Kang, D. W. et al. Emerging porous materials and their composites for NH₃ gas removal. *Adv. Sci.* **7**, 2002142 (2020).
44. Wang, H. et al. Assessment of the performances and reactions of quaternary LC2-slag cement. *Adv. Cem. Res.* **34**, 529–541 (2022).

Acknowledgments

The authors would like to acknowledge the financial supports from the International Cooperation and Exchange of the National Natural Science Foundation of China (Grant no. 52261160646), National Natural Science Foundation of China, Youth Science Foundation Project (Class A) (Grant No. 52525901), National Natural Science Foundation of China (Grant No. 52378224), National Key Research and Development Program of China (Grant no. 2023YFE0205400), The Science and Technology Development Fund, Macao SAR (File no. 0076/2022/AFJ).

Author contributions

Han Wang: Conceptualization, Data curation, Formal analysis, Investigation, Methodology, Writing-original draft. Yanchun Miao: Data curation, Formal analysis, Methodology. TaoTao Feng: Conceptualization, Data curation, Investigation. Junlin Lin: Conceptualization, Supervision, Writing-review & editing. Guoxing Sun: Data curation, Investigation, Methodology, Supervision, Writing-review & editing. Zeyu Lu: Conceptualization, Data curation, Investigation, Methodology, Supervision, Writing-review & editing. Jinyang Jiang: Conceptualization, Supervision, Writing-review & editing.

Competing interests

The authors declare no competing interests.

Additional information

Supplementary information The online version contains supplementary material available at <https://doi.org/10.1038/s44296-025-00072-w>.

Correspondence and requests for materials should be addressed to Zeyu Lu.

Reprints and permissions information is available at <http://www.nature.com/reprints>

Publisher's note Springer Nature remains neutral with regard to jurisdictional claims in published maps and institutional affiliations.

Open Access This article is licensed under a Creative Commons Attribution 4.0 International License, which permits use, sharing, adaptation, distribution and reproduction in any medium or format, as long as you give appropriate credit to the original author(s) and the source, provide a link to the Creative Commons licence, and indicate if changes were made. The images or other third party material in this article are included in the article's Creative Commons licence, unless indicated otherwise in a credit line to the material. If material is not included in the article's Creative Commons licence and your intended use is not permitted by statutory regulation or exceeds the permitted use, you will need to obtain permission directly from the copyright holder. To view a copy of this licence, visit <http://creativecommons.org/licenses/by/4.0/>.

© The Author(s) 2025